

Journal of Materials Chemistry A

Accepted Manuscript



This is an *Accepted Manuscript*, which has been through the Royal Society of Chemistry peer review process and has been accepted for publication.

Accepted Manuscripts are published online shortly after acceptance, before technical editing, formatting and proof reading. Using this free service, authors can make their results available to the community, in citable form, before we publish the edited article. We will replace this *Accepted Manuscript* with the edited and formatted *Advance Article* as soon as it is available.

You can find more information about *Accepted Manuscripts* in the [Information for Authors](#).

Please note that technical editing may introduce minor changes to the text and/or graphics, which may alter content. The journal's standard [Terms & Conditions](#) and the [Ethical guidelines](#) still apply. In no event shall the Royal Society of Chemistry be held responsible for any errors or omissions in this *Accepted Manuscript* or any consequences arising from the use of any information it contains.

ARTICLE

Efficient carrier transport in halide perovskites: theoretical perspectives

Cite this: DOI: 10.1039/x0xx00000x

M. H. Du^aReceived 00th January 2014,
Accepted

DOI: 10.1039/x0xx00000x

www.rsc.org/

Halide perovskites have recently been shown to exhibit excellent carrier transport properties. Density functional calculations are performed to study the electronic structure, dielectric properties, and defect properties of β - $\text{CH}_3\text{NH}_3\text{PbI}_3$. The results show that Pb chemistry plays an important role in a wide range of material properties, i.e., small effective masses, enhanced Born effective charges and lattice polarization, and the suppression of the formation of deep defect levels, all of which contribute to the exceptionally good carrier transport properties observed in $\text{CH}_3\text{NH}_3\text{PbI}_3$. Defect calculations show that the iodine interstitial is the only low-energy native point defect that acts as a deep trap and non-radiative recombination centre. Alloying iodide with chloride reduces the lattice constant of the iodide and significantly increases the formation energy of interstitial defects, which explains the observed substantial increase in carrier diffusion length in mixed halide $\text{CH}_3\text{NH}_3\text{PbI}_2\text{Cl}$ compared to that in $\text{CH}_3\text{NH}_3\text{PbI}_3$.

I. Introduction

Halides are not usually considered as electronic or optoelectronic materials because their transport properties are usually inferior compared to more covalent semiconductors. However, several halide perovskite materials have recently been found to exhibit exceptionally good transport properties (e.g., high mobility, long carrier lifetime and diffusion length) for both electrons and holes.^{1,2} Methylammonium (MA) lead iodide chloride ($\text{CH}_3\text{NH}_3\text{PbI}_{1-x}\text{Cl}_x$) is reported to have electron and hole diffusion lengths both exceeding 1 μm .¹ Halide perovskites (e.g., $\text{CH}_3\text{NH}_3\text{PbI}_3$ and $\text{CH}_3\text{NH}_3\text{PbI}_{1-x}\text{Cl}_x$, CsSnI_3) have been used as medium for electron and/or hole transport in mesostructured solar cells with distributed heterojunctions or in planar heterojunction thin-film solar cells.^{4,5,6,7,8} Recent experiments showed impressive solar energy conversion efficiency of over 15% for $\text{CH}_3\text{NH}_3\text{PbI}_{3-x}\text{Cl}_x$ -based planar heterojunction thin solar cells.⁷ Good transport properties of halide perovskites also find applications in other areas. CsPbBr_3 has been discovered as a promising room-temperature γ -ray detector material with high electron and hole mobility-lifetime products ($\mu\tau$), which are 1.7×10^{-3} and 1.3×10^{-3} cm^2/V , respectively.³ A long electron lifetime of 2.5 μs was observed for CsPbBr_3 . Remarkably, these halide perovskites show good bi-polar conduction, which is not often found in compound semiconductors, especially not in halides.

Density functional calculations have been performed to study the electronic structure of $\text{CH}_3\text{NH}_3(\text{Pb},\text{Sn})\text{X}_3$ and $\text{Cs}(\text{Pb},\text{Sn})\text{X}_3$ ($\text{X} = \text{Cl}, \text{Br}, \text{I}$).^{9,10,11,12,13,14} The calculated band structure of these compounds generally shows large dispersion for both conduction and valence bands and consequently small effective masses for both electrons and holes.^{9,10,11,12} The electron and hole effective masses of α - $\text{CH}_3\text{NH}_3\text{PbI}_3$ (pseudo-cubic high-temperature phase)^{15,16} were calculated to be 0.23 m_0 and 0.29 m_0 , respectively, along the R- Γ direction,¹² consistent with the good bi-polar conduction observed experimentally.^{1,2} Recent defect calculations of α - $\text{CH}_3\text{NH}_3\text{PbI}_3$ show that low-energy native point defects create only shallow levels,

which are not effective carrier traps.¹⁷ Similar defect properties have also been reported for other halides (e.g., TlBr) that exhibit excellent transport properties based on density functional calculations.¹⁸

Recent experiments show that the electron and hole diffusion lengths of the mixed halides ($\text{CH}_3\text{NH}_3\text{PbI}_2\text{Cl}$) are nearly one order of magnitude longer than those of their triiodide counterpart ($\text{CH}_3\text{NH}_3\text{PbI}_3$).^{1,2} Cl is more ionic than I and carrier transport, especially hole transport, in chlorides is usually less efficient than in iodides. Previous calculations on CsSnX ($\text{X} = \text{Cl}, \text{Br}, \text{I}$) show that the hole effective mass increases from chloride to bromide and iodide as expected.⁹ It is therefore puzzling why the electron and hole diffusion lengths of the mixed halides are substantially longer than those of triiodides.

In this paper, electronic structure, dielectric properties, and defect properties of β - $\text{CH}_3\text{NH}_3\text{PbI}_3$ (tetragonal room-temperature phase)^{15,16} are studied to understand the efficient carrier transport in halide perovskites. Chemistry of ns^2 cations (which have the outer electronic configuration of ns^2 , e.g., Pb^{2+} , Sn^{2+} , Tl^+ , and Bi^{3+}) plays an important role in the electronic and dielectric properties of halide perovskites containing ns^2 cations, such as $\text{CH}_3\text{NH}_3\text{PbI}_3$. In $\text{CH}_3\text{NH}_3\text{PbI}_3$, the conduction band is derived from the spatially extended Pb-6p states, resulting in significant cross-bandcap hybridization, which enhances covalency and Born effective charges. Enhanced covalency increases carrier velocity. Enhanced Born charge leads to large static dielectric constant, which reduces carrier scattering and trapping at charged defects and impurities. Furthermore, among all the native point defects (including vacancies, interstitials, and antisites), only iodine interstitial is found to induce deep trapping levels and act as a nonradiative recombination centre. This is in contrast to previous calculations that show the iodine interstitial as a shallow acceptor.¹⁷ Although the iodine interstitial is a deep trap, the electron or hole trapping at an iodine interstitial should be subject to a kinetic barrier, thereby limiting the trapping cross-section. Mixing iodide with chloride reduces the lattice constant of the iodide and thus suppresses the

formation of interstitials, including the iodine interstitial. This can explain the observed increased carrier diffusion lengths in mixed halides compared to those in triiodides.

We have reported the electronic structure, dielectric properties, and defect properties for a large number of halides that contain ns^2 cations,^{18,19,20,21} such as TlBr and Tl₆SeI₄,^{22,23} which exhibit efficient electron transport ($\mu\tau_e \sim 10^{-3}$ cm²/V and $\tau_e > 1$ μ s). The present study of halide perovskites provides further evidence that the favourable electronic and dielectric properties involving chemistry of ns^2 cations and the lack of effective carrier traps are the main factors that lead to the excellent transport properties in halides that contain ns^2 cations.

II. Computational Methods

Density functional theory (DFT)²⁴ with standard Perdew-Burke-Ernzerhof (PBE)²⁵ functionals were used to calculate electronic structure, Born effective charges, dielectric constant, and defect properties of β -CH₃NH₃PbI₃ and CH₃NH₃PbI₂Cl. Heyd-Scuseria-Ernzerhof (HSE) hybrid functional²⁶ calculations were also performed on the defects that insert deep defect levels in the band gap. 43% non-local Fock exchange was used to produce a direct band gap (at Γ point) of 1.50 eV, close to the experimental band gap of 1.51-1.52 eV.^{15,16} The structures optimized at the PBE level were used for the HSE calculations. The PBE calculations provide sufficiently accurate results on forces (near equilibrium), structures, and band dispersion, but underestimates band gaps (see Table I).²⁷ The HSE calculations were performed to correct the band gap and to determine the positions of the deep defect levels relative to valence and conduction band edges. Experimental lattice parameters were used in all calculations for both CH₃NH₃PbI₃ (tetragonal: $a = 8.849$ Å, $c = 12.642$ Å)¹⁶ and CH₃NH₃PbI₂Cl (orthorhombic: $a = 8.825$ Å, $b = 8.835$ Å, $c = 11.24$ Å).⁶

Table I. Band gaps of CH₃NH₃PbI₃ and CH₃NH₃PbI₂Cl calculated using PBE and HSE functionals. Spin-orbit coupling is included in the calculations. The units are in eV.

	CH ₃ NH ₃ PbI ₃	CH ₃ NH ₃ PbI ₂ Cl
PBE	0.60	0.78
HSE	1.50	1.76
Exp.	1.51 (Ref. 15); 1.52 (Ref. 16)	

The electron-ion interactions were described using projector augmented wave potentials.²⁸ PBE pseudopotentials were used for both PBE and HSE calculations. The numbers of valence electrons for Pb, I, C, N, H that were included in the calculations are 14, 7, 4, 5, and 1, respectively. The valence wavefunctions were expanded in a plane-wave basis with cut-off energy of 400 eV. All atoms were relaxed to minimize the Feynman-Hellmann forces to below 0.05 eV/Å. For calculations of Born effective charges and dielectric constants, the cut-off energy of 500 eV was used and the forces were minimized to below 0.01 eV/Å. All calculations were performed using the VASP codes.^{29,30}

A $2 \times 2 \times 1$ tetragonal supercell containing 16 formula units of CH₃NH₃PbI₃ was used to study native point defects in β -CH₃NH₃PbI₃. A $1 \times 1 \times 2$ grid was used for k-point sampling of Brillouin zone. The charge transition level $\varepsilon(q/q')$ for a defect is determined by the Fermi level (ε_f) at which the formation energies of the defect with charge states q and q' are equal to each other. $\varepsilon(q/q')$ can be calculated using

$$\varepsilon(q/q') = \frac{E_{D,q'} - E_{D,q}}{q - q'} \quad (1)$$

where $E_{D,q}$ ($E_{D,q'}$) is the total energy of the supercell that contains the relaxed structure of a defect at charge state q (q'). Details on the calculations of defect formation energies and transition levels can be found in Refs. 31 and 32. Tests on different cutoff energies and k-point meshes show that the calculated defect transition levels are converged to better than 0.1 eV. Spin-orbit coupling (SOC) was included in all calculations except those for Born effective charges and dielectric constant. SOC has a large impact on the electronic structure of heavy 6p ions^{9,10,11,12,19} but its effects on forces and Born effective charges are usually insignificant.³³

III. Results and Discussion

A. Electronic structure and dielectric properties

The structure of β -CH₃NH₃PbI₃ has been determined experimentally to be body-centered tetragonal (space group $I4cm$)¹⁶ with PbI₆ octahedra tilted along the c axis [Figures 1(a) and (b)]. The octahedra on two adjacent layers tilt in opposite directions (out of phase). The (CH₃NH₃)⁺ cations can freely rotate at room temperature,¹⁵ which makes the body-centered tetragonal structure possible. However, in calculations, the (CH₃NH₃)⁺ cations have to be relaxed to fixed orientations as shown in Figure 1, which reduces the symmetry to simple tetragonal. The calculations show that the (CH₃NH₃)⁺ cations prefer to lie on the ab plane with its C-N bond aligned approximately with $[110]$ or $[\bar{1}\bar{1}0]$ direction.

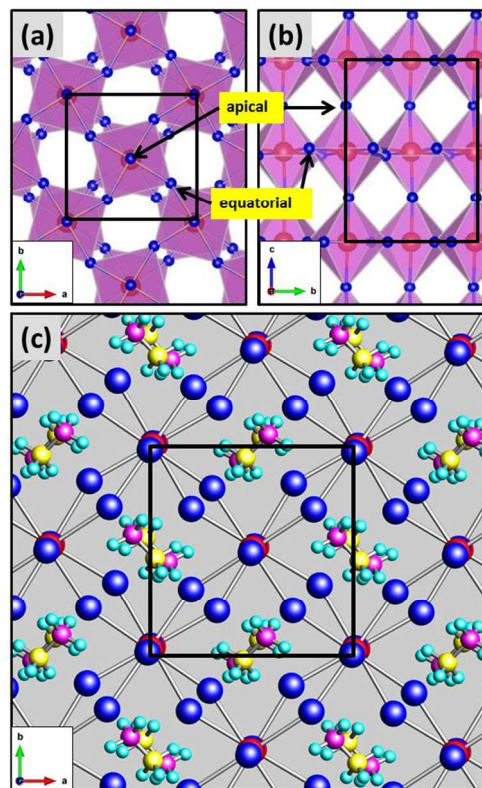


Figure 1. Tetragonal perovskite structure with out-of-phase tilting of the PbI₆ octahedra around the c axis viewed from $[001]$ (a) and $[100]$ (b) directions. The equatorial and apical sites of the iodine ions in a PbI₆ octahedron are also shown. (The equatorial and apical iodine ions are bonded with Pb ions on the ab plane and along the c axis, respectively.) The (CH₃NH₃)⁺ ions are not shown in (a) and (b) for clarity. (c) Ball-and-stick plot of β -CH₃NH₃PbI₃ ($[001]$ view).

Figure 2 shows the band structure of β - $\text{CH}_3\text{NH}_3\text{PbI}_3$ calculated using PBE functionals. The PBE calculation shows a direct band gap of 0.60 eV at Γ point. The underestimation of the band gap (compared to the experimentally measured band gap of 1.51-1.52 eV^{15,16}) is a well-known problem of PBE functionals. The inclusion of the SOC lowers the band gap by nearly 1 eV mostly by lowering the CBM, consistent with previous calculations.^{10,11} The SOC has also been found to be important in other compounds containing heavy 6p cations, such as in TlBr.¹⁹ Both conduction and valence bands near band edges are very dispersive. The calculated electron and hole effective masses are $m_{e,x} = 0.32 m_0$, $m_{h,x} = 0.37 m_0$ along the Γ -X direction and $m_{e,z} = 0.20 m_0$, $m_{h,z} = 0.27 m_0$ along the Γ -Z direction (see Table II), close to those calculated for α - $\text{CH}_3\text{NH}_3\text{PbI}_3$.¹² The larger effective masses along the x/y direction are likely due to the larger distortion of the Pb-I-Pb angles as a result of the tilting of the PbI_6 octahedrons.

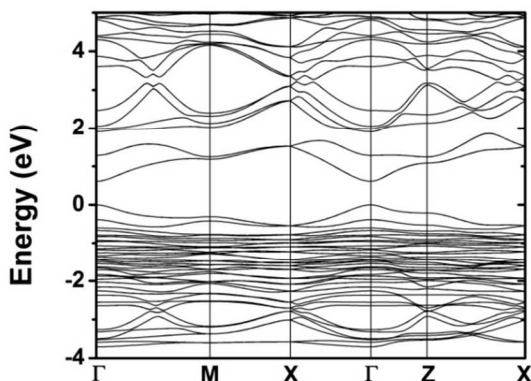


Figure 2. Band structure of β - $\text{CH}_3\text{NH}_3\text{PbI}_3$ calculated using PBE functionals. The energy of valence band maximum is set to zero.

Table II. Calculated electron and hole effective masses for tetragonal $\text{CH}_3\text{NH}_3\text{PbI}_3$ and orthorhombic $\text{CH}_3\text{NH}_3\text{PbI}_2\text{Cl}$.

	$\text{CH}_3\text{NH}_3\text{PbI}_3$	$\text{CH}_3\text{NH}_3\text{PbI}_2\text{Cl}$
$m_{e,x}$	0.32	0.30
$m_{e,y}$	0.32	0.25
$m_{e,z}$	0.20	0.77
$m_{h,x}$	0.37	0.29
$m_{h,y}$	0.37	0.28
$m_{h,z}$	0.27	1.25

Density of states (DOS) of β - $\text{CH}_3\text{NH}_3\text{PbI}_3$ is shown in Figure 3. There are two Pb-6s peaks located between -8.5 and -6.5 eV and right below the valence band maximum (VBM) in DOS figure (Figure 3). They overlap with I-5p states, indicating significant hybridization between the Pb-6s and the I-5p states. Such hybridization contributes to the large dispersion of the valence band. The conduction band is derived from Pb-6p states, which are spatially more extended than the usual s- or d-state-derived conduction band in compound semiconductors. The Pb-6p and I-5p orbitals point to each other, leading to enhanced hybridization. Significant cross-bandgap hybridization between the Pb-6p and the I-5p states can be seen in DOS in Fig. 2 as evidenced by the overlap between the Pb-6p and I-5p states in both conduction and valence bands. The mixed ionic-covalent character is known to give rise to enhanced Born effective charges (which reflects enhanced lattice polarization in response to the displacement of ions) in ferroelectric oxides, such as PbTiO_3 ,^{34 35 36 37} and in halides containing ns² cations, such as Tl, In, Pb, and Bi halides.^{19,20,21,38} Indeed, enhanced Born effective charges are found for $\text{CH}_3\text{NH}_3\text{PbI}_3$. β - $\text{CH}_3\text{NH}_3\text{PbI}_3$ has body-centred tetragonal structure, which implies that $(\text{CH}_3\text{NH}_3)^+$

ions must freely rotate and take random orientations. In the ideal body-centred tetragonal structure (space group $I4cm$) of β - $\text{CH}_3\text{NH}_3\text{PbI}_3$, Z_{xz}^* , Z_{yx}^* , Z_{yz}^* , and Z_{xy}^* of the Born effective charge tensor should be zero. However, in calculations, $(\text{CH}_3\text{NH}_3)^+$ ions are relaxed into fixed configurations, which lower the symmetry. As a result, the calculated Born charges in $\text{CH}_3\text{NH}_3\text{PbI}_3$ show differences on lattice sites that should be equivalent in $I4cm$ structure and Z_{xz}^* , Z_{yx}^* , Z_{yz}^* , and Z_{xy}^* are nonzero. For simplicity, $(\text{CH}_3\text{NH}_3)^+$ is replaced by a uniform positive charge background with total charge equal to that of the $(\text{CH}_3\text{NH}_3)^+$ ions. The resulting Born effective charges are shown in Table III. If the $(\text{CH}_3\text{NH}_3)^+$ ions are explicitly included, the Born effective charges (Z_{xx}^* , Z_{yy}^* , and Z_{zz}^*) averaged over the lattice sites that are equivalent under $I4cm$ symmetry are very close to those shown in Table III (e.g., averaged Z_{xx}^* , Z_{yy}^* , and Z_{zz}^* are 4.35, 4.35, and 4.69, respectively, for Pb in β - $\text{CH}_3\text{NH}_3\text{PbI}_3$). This is not surprising since the enhancement in Born effective charges is mainly due to the mixed ionic-covalent character of the Pb-I bonds.

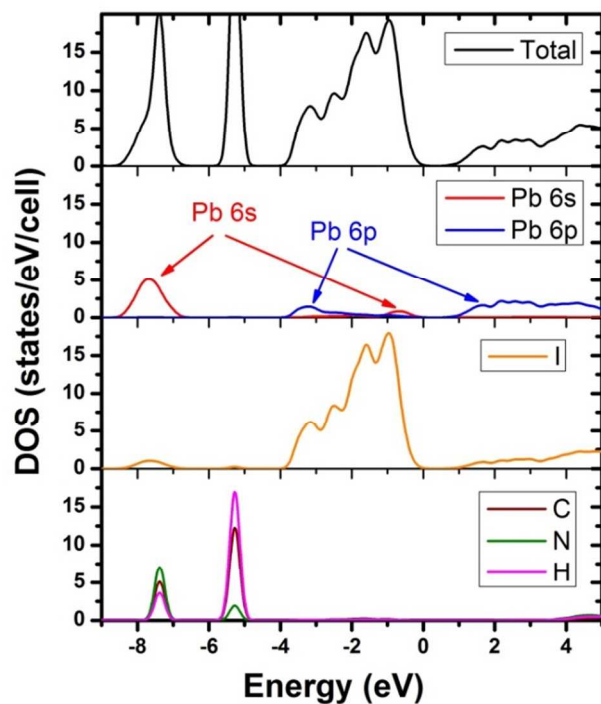


Figure 3. Density of states (DOS) of β - $\text{CH}_3\text{NH}_3\text{PbI}_3$ calculated using PBE functionals. The total DOS is projected into Pb (6s and 6p), I, C, N, and H atoms. The energy of valence band maximum is set to zero.

The Born effective charges for Pb are more than doubled from its nominal ionic charge of +2. The Pb- I_{4a} bond is aligned with the c axis. Thus, Z_{zz}^* for apical iodine ions (I_{4a}) is significantly enhanced by more than a factor of 3. For equatorial iodine ions, the Born charge enhancement is found on the ab plane where Pb- I_{8c} bonds lie. (The equatorial and apical iodine ions are bonded with Pb ions on the ab plane and along the c axis, respectively, as shown in Figure 1.)

The enhanced Born effective charges in $\text{CH}_3\text{NH}_3\text{PbI}_3$ lead to relatively large static dielectric constant in which the lattice contribution is much larger than the electronic contribution. The

calculated static dielectric tensor with $(\text{CH}_3\text{NH}_3)^+$ ions explicitly included in the calculation is $\epsilon_0^{xx} = 25.40$, $\epsilon_0^{yy} = 21.88$, $\epsilon_0^{zz} = 17.83$, $\epsilon_\infty^{xx} = 5.30$, $\epsilon_\infty^{yy} = 5.27$ and $\epsilon_\infty^{zz} = 4.62$, where ϵ_0 and ϵ_∞ are static and optical dielectric constants, respectively. ϵ_0^{xx} and ϵ_∞^{xx} differ from ϵ_0^{yy} and ϵ_∞^{yy} , respectively, due to fixing the orientations of $(\text{CH}_3\text{NH}_3)^+$ ions, which reduces the symmetry. It is clear that the static dielectric constant is large (~ 20) compared to most of the compound semiconductors with similar band gaps and the dielectric screening is dominated by lattice (rather than electron) polarization.

Table III. Born effective charge (Z^*) tensors (Cartesian coordinates) for β - $\text{CH}_3\text{NH}_3\text{PbI}_3$ with $(\text{CH}_3\text{NH}_3)^+$ ions replaced by a uniform charge background (space group $I4cm$). The Wyckoff positions (WP) are shown and only the charges for the inequivalent atoms are listed.

Atom Type	WP	Born effective charge tensor
Pb	4a	$\begin{pmatrix} 4.38 & -0.84 & 0.0 \\ 0.84 & 4.38 & 0.0 \\ 0.0 & 0.0 & 4.86 \end{pmatrix}$
I (apical)	4a	$\begin{pmatrix} -0.53 & 0.0 & 0.0 \\ 0.0 & -0.53 & 0.0 \\ 0.0 & 0.0 & -3.45 \end{pmatrix}$
I (equatorial)	8c	$\begin{pmatrix} -2.43 & 1.79 & 0.0 \\ 1.79 & -2.43 & 0.0 \\ 0.0 & 0.0 & -0.61 \end{pmatrix}$

The large static dielectric constant provides effective screening of the charged defects and impurities, thereby reducing the carrier scattering and trapping and consequently increasing the carrier lifetime and diffusion length. On the other hand, strong screening should also generally reduce the formation energy of charged defects because the Coulomb potential applied by the charged defect on the rest of the crystal lattice is strongly screened. However, the low defect formation energy can be largely remedied if the material synthesis temperature is low. The halide perovskites used in solar cells are synthesized at low temperatures (e.g., 100 °C for solution-based growth⁶). Low growth temperature can suppress the defect formation despite having low defect formation energy. Therefore, a combination of large static dielectric constant and low temperature material synthesis can effectively suppress the carrier scattering and trapping by charged defects and impurities.

The calculation of the static dielectric constant does not consider the reorientation of the $(\text{CH}_3\text{NH}_3)^+$ ions, which possess electric dipole moments.³⁹ It is known that these ions can freely rotate at room temperature.¹⁵ Therefore, the $(\text{CH}_3\text{NH}_3)^+$ ions should reorient in response to a charged defect and provide additional screening. However, the $(\text{CH}_3\text{NH}_3)^+$ ions are unlikely to rotate fast enough to respond to a diffusing electron or hole because otherwise they will provide an attractive potential that turns a free carrier to a polaron, which has not been observed experimentally.

B. Defects

Although charged defects are screened by the large static dielectric constant in $\text{CH}_3\text{NH}_3\text{PbI}_3$, they still play an important role in carrier scattering and trapping. The defects that introduce deep levels in the band gap are particularly detrimental to the carrier transport because they are effective carrier traps and non-radiative

recombination centres. Defect levels in β - $\text{CH}_3\text{NH}_3\text{PbI}_3$ are studied in details here. Native point defects, including vacancies (V_{MA} , V_{Pb} , V_{I}), interstitials (MA_i , Pb_i , I_i), and antisites (Pb_{MA} , MA_{Pb} , Pb_{I} , MA_{I} , I_{Pb} , I_{MA}) are considered in the calculations. Remarkably, among all these native point defects, only I_i is found to be a deep carrier trap and non-radiative recombination centre. All the vacancies (V_{MA} , V_{Pb} , V_{I}), cation interstitials (MA_i , Pb_i), and some antisite defects (MA_i , Pb_{MA} , MA_{Pb}) create only shallow levels. Specifically, V_{I} , MA_i , Pb_i , MA_i , Pb_{MA} are shallow donors while V_{MA} , V_{Pb} , and MA_{Pb} are shallow acceptors. I_{Pb} (I_{MA}) spontaneously transforms into V_{Pb} (V_{MA}) and I_i during structural relaxation. Similarly, Pb_i is unstable against dissociation to form Pb_i and V_{I} . I_{Pb} , I_{MA} , and Pb_i are unstable both energetically and kinetically.

I_i was found to be a low-energy defect in α - $\text{CH}_3\text{NH}_3\text{PbI}_3$. Since the phase transition from α to β phase of $\text{CH}_3\text{NH}_3\text{PbI}_3$ takes place at a low temperature of about 60 °C,¹⁵ the low-energy defects found in α - $\text{CH}_3\text{NH}_3\text{PbI}_3$ should freeze in the lattice and remain to be the dominant defects in β - $\text{CH}_3\text{NH}_3\text{PbI}_3$.¹⁷

I_i is stable as a split interstitial, where two I atoms occupy one I site. I_i has two stable charge states, i.e., +1 and -1. I_i^+ can be considered as a neutral I_2 molecule inside a V_{I}^+ [Figure 4(a)]. There is some hybridization between the antibonding orbital of the I_2 molecule and the 5p states of the nearby iodine anions. Adding two electrons into I_i^+ breaks the I-I bond and therefore I_i^- can be considered as two Γ^- ions bound in V_{I}^- [Figure 4(b)]. Neutral I_i^0 is metastable because I_i is a negative- U centre and its (+/-) transition level is located between its (+/0) and (0/-) levels calculated using Eq. 1. I_i can be on either apical or equatorial site of the PbI_6 octahedron in β - $\text{CH}_3\text{NH}_3\text{PbI}_3$. Figure 4 shows the structures of I_i^+ and I_i^- on the equatorial site. The structures of I_i^+ and I_i^- on the apical site are similar to those on the equatorial site. The PBE (HSE) calculations including SOC find that I_i^+ is more stable on the equatorial site than on the apical site by 0.09 (0.06) eV whereas I_i^- is more stable on the apical site than on the equatorial site by 0.15 (0.19) eV. (The HSE calculations used the PBE optimized structures.) The HSE calculations show that the transition between I_i^+ (equatorial) and I_i^- (apical) occurs at $\epsilon_{\text{VBM}} + 0.54$ eV (see Figure 5). The electron trapping level, the (+/0) level, on equatorial I_i^+ is calculated to be $\epsilon_{\text{VBM}} + 0.88$ eV and the hole trapping level, (0/-) level, on apical I_i^- is calculated to be $\epsilon_{\text{VBM}} + 0.18$ eV. The (+/0) level is a deep trapping level and a non-radiative recombination level.

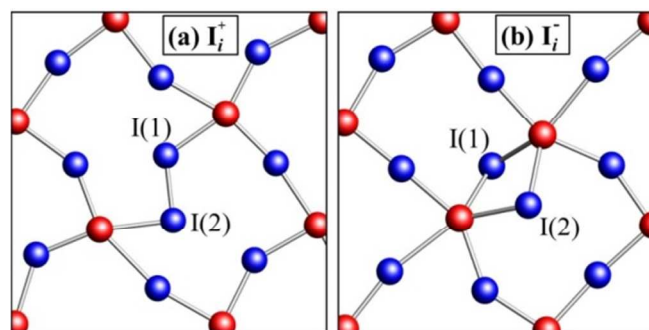


Figure 4. Structures of iodine split interstitials on the equatorial site at +1 (a) and -1 (b) charge states, respectively. The atoms I(1) and I(2) are the two iodine atoms that occupy the same iodine lattice site. Note that only one layer of Pb-I bonding network is shown for clarity.

Although the thermodynamic transition levels of I_i are inside the band gap, there are no single-particle levels of either I_i^+ or I_i^- inside the band gap. This is observed in both PBE and HSE calculations including SOC. For example, for an apical I_i^+ , the empty single-particle I-I antibonding orbital is located at about 0.26 eV above the CBM at the HSE level. For an apical I_i^- , the occupied single-particle levels of the two Γ ions are below the VBM, mixing with the valence band states. The supercell employed in this work is still not sufficiently large to resolve the positions of the localized Γ states at I_i^- . The (+/0) and (0/-) thermodynamic transition levels are inside the band gap due to the large structural relaxation when changing the charge state from either +1 or -1 to neutral. The I-I distance at the apical I_i changes from 3.10 to 3.61, and 3.81 Å when its charge state changes from +1 to neutral and -1. The absence of the single-particle defect levels in the band gap suggests that the electron and hole trapping involves kinetic barriers, which should lead to reduced capture cross-section, although the trapping is energetically favourable.

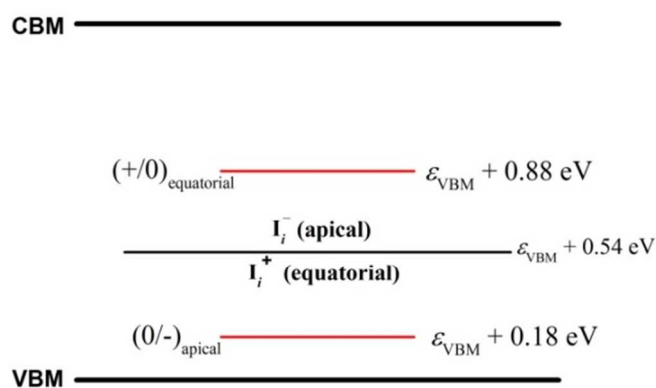


Figure 5. Iodine interstitial induced defect levels in β - $\text{CH}_3\text{NH}_3\text{PbI}_3$. I_i^+ on the equatorial site and I_i^- on the apical site are stable when the Fermi level is above and below $\epsilon_{\text{VBM}} + 0.54$ eV, respectively. I_i^+ (equatorial) can trap an electron at its (+/0) level, i.e., $\epsilon_{\text{VBM}} + 0.54$ eV. I_i^- (apical) can trap a hole at its (0/-) level, i.e., $\epsilon_{\text{VBM}} + 0.18$ eV.

Small polarons are often found in cation vacancies in ionic compounds. However, the hole localization is not found in cation vacancies in $\text{CH}_3\text{NH}_3\text{PbI}_3$ in both PBE and HSE calculations. This is likely due to the strong hybridization between the Pb-6s states and the I-5p states near the VBM, which delocalizes the VBM states and increases the energy cost for hole localization. This is consistent with the previous results that show no hole localization in V_{Tl} in TlBr (a more ionic material with a larger 2.68-eV band gap) due to the hybridization between the Tl-6s and Br-4p states near VBM.¹⁸

The anion vacancy (V_i) is found to be a shallow donor, in contrast to the frequently seen anion-vacancy-induced F -centre level in alkali halides. Adding more electrons to the supercell that contains V_i^+ leads to the filling of the delocalized bulk CBM states in both PBE and HSE calculations including SOC. This is likely related to the spatially more extended Pb-6p orbitals around V_i in $\text{CH}_3\text{NH}_3\text{PbI}_3$ in contrast to the cation-s orbitals around the F -centres in alkali halides.

Pb_i^{2+} is most stable when binding with four iodine ions on the ab plane. Adding electrons to the supercell that contains Pb_i^{2+} leads to the filling of the delocalized bulk CBM states in PBE calculations

including SOC. The Pb 6p states of Pb_i are above the CBM calculated using hybrid functional calculations including SOC. Therefore, band gap correction by hybrid functional calculations should not change the shallow donor nature of Pb_i . Ref. 17 shows Pb_i as a deep donor due perhaps to the neglecting of SOC in the calculations, which artificially raises the CBM.

The defect calculations show that the native point defects in $\text{CH}_3\text{NH}_3\text{PbI}_3$ are benign in terms of carrier trapping. Most of the native point defects create only shallow levels. The iodine interstitial is the only deep trap found among all the native point defects (including vacancies, interstitials, and antisites) and therefore should play a very important role in carrier trapping and recombination. However, even the trapping at the iodine interstitial is subject to a kinetic barrier, thereby limiting the trapping cross-section. These results are consistent with the experimentally observed long electron and hole diffusion length (~ 100 nm) in $\text{CH}_3\text{NH}_3\text{PbI}_3$.^{1,2}

C. $\text{CH}_3\text{NH}_3\text{PbI}_3$ vs. $\text{CH}_3\text{NH}_3\text{PbI}_2\text{Cl}$

The electron and hole diffusion lengths in $\text{CH}_3\text{NH}_3\text{PbI}_3$ have been shown to increase by about a factor of ten when mixing iodide and chloride in the form of $\text{CH}_3\text{NH}_3\text{PbI}_{3-x}\text{Cl}_x$ ($x \approx 1$).¹ Carrier velocity is expected to be reduced when mixing iodide with chloride. However, if carrier trapping can be suppressed by alloying, the carrier diffusion length can be increased. The results from the defect calculations of native point defects show that only the iodine interstitial is a deep trap while others are shallow donors or acceptors. By alloying iodide with chloride, the lattice constant is reduced, which should suppress the formation of interstitial defects, thereby reducing the density of trapping levels induced by iodine interstitials.

$\text{CH}_3\text{NH}_3\text{PbI}_2\text{Cl}$ has an orthorhombic perovskite structure with lattice parameters $a = 8.825$ Å, $b = 8.835$ Å, $c = 11.24$ Å.⁶ Compared to $\text{CH}_3\text{NH}_3\text{PbI}_3$ ($a = 8.849$ Å, $c = 12.642$ Å),¹⁶ the lattice constant along c axis is significantly reduced in $\text{CH}_3\text{NH}_3\text{PbI}_2\text{Cl}$. This is consistent with the previous DFT calculations, which show that the Cl atoms preferentially occupy the apical sites in the PbI_4Cl_2 octahedra.¹³ $\text{CH}_3\text{NH}_3\text{PbI}_2\text{Cl}$ is studied here with Cl atoms placed on the apical sites and the lattice parameters reported in Ref. 6 were used. The band structure and the DOS of $\text{CH}_3\text{NH}_3\text{PbI}_2\text{Cl}$ calculated using PBE functionals are shown in Figures 6 and 7, respectively. The addition of Cl introduces Cl 3p states in the lower portion of the valence band as shown in Figure 7. The valence band edge is still made up of predominately I-5p states. The band gap of $\text{CH}_3\text{NH}_3\text{PbI}_2\text{Cl}$ is calculated to be 1.76 eV using HSE calculations including SOC, which is larger than the calculated band gap of 1.50 eV for $\text{CH}_3\text{NH}_3\text{PbI}_3$ (see Table I). Since the Cl atoms are placed on the apical sites, the electron and hole effective masses in the z direction of $\text{CH}_3\text{NH}_3\text{PbI}_2\text{Cl}$ are increased significantly from those of $\text{CH}_3\text{NH}_3\text{PbI}_3$ as shown in Table II. On the ab plane, the carrier transport is still conducted in the Pb-I bonding network. Therefore, the electron and hole effective masses on the x and y directions of $\text{CH}_3\text{NH}_3\text{PbI}_2\text{Cl}$ do not change much from those of $\text{CH}_3\text{NH}_3\text{PbI}_3$. They actually decrease slightly due to the reduced lattice constant in $\text{CH}_3\text{NH}_3\text{PbI}_2\text{Cl}$ that enhances hybridization and carrier velocity in the ab plane. Unlike ordered Cl distribution (on apical sites) in the calculations, there should be disorder in Cl distribution in real materials. The average carrier velocity in $\text{CH}_3\text{NH}_3\text{PbI}_{3-x}\text{Cl}_x$ should be lower than that in $\text{CH}_3\text{NH}_3\text{PbI}_3$ due to the more localized Cl-3p states than I-5p states.

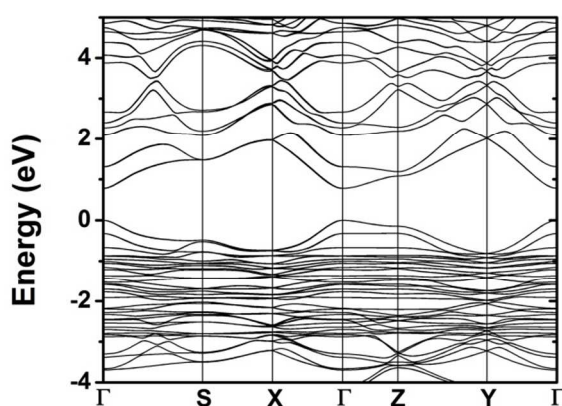


Figure 6. Band structure of β - $\text{CH}_3\text{NH}_3\text{PbI}_2\text{Cl}$ calculated using PBE functionals. The energy of valence band maximum is set to zero.

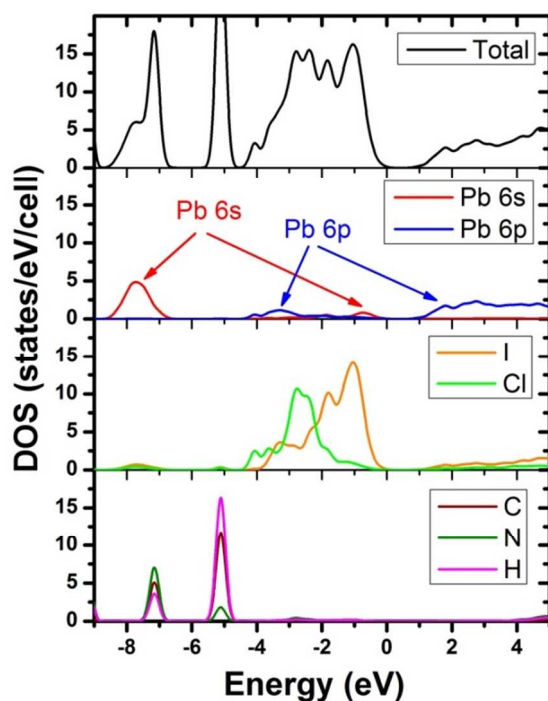


Figure 7. Density of states (DOS) of β - $\text{CH}_3\text{NH}_3\text{PbI}_2\text{Cl}$ calculated using PBE functionals. The total DOS is projected into Pb (6s and 6p), I, Cl, C, N, and H atoms. The energy of valence band maximum is set to zero.

Since the iodine interstitial is the only deep trap in $\text{CH}_3\text{NH}_3\text{PbI}_3$, it is studied in details for $\text{CH}_3\text{NH}_3\text{PbI}_2\text{Cl}$. An interstitial iodine atom prefers to form a split interstitial with another iodine atom on the equatorial site in $\text{CH}_3\text{NH}_3\text{PbI}_2\text{Cl}$. Assuming similar growth conditions for $\text{CH}_3\text{NH}_3\text{PbI}_3$ and for $\text{CH}_3\text{NH}_3\text{PbI}_2\text{Cl}$ and the Fermi levels in the two materials are equal to each other on absolute scale, or in other words, their work functions are the same, the formation energy of an iodine interstitial defect in $\text{CH}_3\text{NH}_3\text{PbI}_2\text{Cl}$ is higher than that in $\text{CH}_3\text{NH}_3\text{PbI}_3$ by 0.66 eV for I_i^+ and by 0.43 eV for I_i^- .³¹

³² These are calculated using PBE functionals without SOC since SOC does not affect energetics significantly. If comparing neutral I_i^0 in two materials (so that the Fermi level is not involved when calculating the defect formation energy difference^{31, 32}), the formation energy of I_i^0 in $\text{CH}_3\text{NH}_3\text{PbI}_2\text{Cl}$ is higher than that in

$\text{CH}_3\text{NH}_3\text{PbI}_3$ by 0.74 eV. Similarly, the formation energies of MA_i^+ and Pb_i^{2+} also increase by 0.99 eV and 0.34 eV when going from $\text{CH}_3\text{NH}_3\text{PbI}_3$ to $\text{CH}_3\text{NH}_3\text{PbI}_2\text{Cl}$. Although MA_i^+ and Pb_i^{2+} are not deep electron traps, they act as scattering centres for carriers. The formation energy increase for the interstitial defects in $\text{CH}_3\text{NH}_3\text{PbI}_2\text{Cl}$ relative to those in $\text{CH}_3\text{NH}_3\text{PbI}_3$ are significant given that the material growth temperature is low (only 100 °C -150 °C).⁶ Clearly, mixing iodide with chloride in the 2:1 ratio suppresses the formation of interstitials and reduces the density of the interstitial-induced scattering centres and deep traps. This should contribute to higher carrier mobility and lifetime.

Next, we estimate the formation energy of Cl interstitial relative to that of I interstitial in $\text{CH}_3\text{NH}_3\text{PbI}_2\text{Cl}$. The purpose is to estimate whether the reduction of the iodine interstitial concentration, $[\text{I}_i]$, is compensated by the increase of the chlorine interstitial concentration, $[\text{Cl}_i]$. The Cl interstitial is found to form Cl-I split interstitial preferably on the equatorial site. The formation energy difference between the Cl_i and I_i of the same charge state in $\text{CH}_3\text{NH}_3\text{PbI}_2\text{Cl}$ can be calculated using

$$\Delta H_f(\text{Cl}_i) - \Delta H_f(\text{I}_i) = E(\text{Cl}_i) - E(\text{I}_i) - \mu_{\text{Cl}} + \mu_{\text{I}}, \quad (2)$$

where $E(\text{Cl}_i)$ and $E(\text{I}_i)$ are the total energies of the supercells that contain a Cl_i and a I_i , respectively. μ_{Cl} and μ_{I} are the chemical potentials of Cl and I, respectively, which are unknown. The formation energy of a substitutional Cl on I site should be positive, i.e.,

$$\Delta H_f(\text{Cl}_i) = E(\text{Cl}_i) - E(\text{bulk}) - \mu_{\text{Cl}} + \mu_{\text{I}} > 0, \quad (3)$$

where $E(\text{bulk})$ and $E(\text{Cl}_i)$ are the total energies of the defect-free supercell and the supercell that contains a Cl_i defect, respectively. Combining Eqs. (2) and (3), one obtains

$$\Delta H_f(\text{Cl}_i) - \Delta H_f(\text{I}_i) > E(\text{Cl}_i) - E(\text{I}_i) - E(\text{Cl}_i) + E(\text{bulk}), \quad (4)$$

Using Eq. 4, one obtains $\Delta H_f(\text{Cl}_i^+) - \Delta H_f(\text{I}_i^+) > 0.14$ eV and $\Delta H_f(\text{Cl}_i^-) - \Delta H_f(\text{I}_i^-) > -0.39$ eV. Therefore, $[\text{Cl}_i^+]$ should be lower than $[\text{I}_i^+]$ and $[\text{Cl}_i^-]$ is possible to be higher than $[\text{I}_i^-]$ in $\text{CH}_3\text{NH}_3\text{PbI}_2\text{Cl}$.

The (+/-) transition level for Cl_i in $\text{CH}_3\text{NH}_3\text{PbI}_2\text{Cl}$ is $\varepsilon_{\text{VBM}} + 0.29$ eV. The neutral Cl_i is metastable. The (+/0) and (0/-) levels are $\varepsilon_{\text{VBM}} + 0.89$ eV and $\varepsilon_{\text{VBM}} - 0.32$ eV, respectively. These transition levels were all calculated using hybrid functional calculations including SOC.

$[\text{I}_i]$ in $\text{CH}_3\text{NH}_3\text{PbI}_2\text{Cl}$ are substantially lower than that in $\text{CH}_3\text{NH}_3\text{PbI}_3$. Based on the results shown above, it can be seen that the introduction of Cl_i in $\text{CH}_3\text{NH}_3\text{PbI}_2\text{Cl}$ cannot compensate the reduction of I_i -induced deep-trap density. Cl_i^+ should have a small impact on the carrier transport because $[\text{Cl}_i^+] < [\text{I}_i^+]$ in $\text{CH}_3\text{NH}_3\text{PbI}_2\text{Cl}$. The formation energy increase for I_i^- due to mixing iodide with chloride is 0.43 eV. The formation energy of Cl_i^- is possibly lower than that of I_i^- in $\text{CH}_3\text{NH}_3\text{PbI}_2\text{Cl}$ but by 0.39 eV at most. Therefore, Cl_i^- may partially compensate the reduction of $[\text{I}_i^-]$. However, the (0/-) hole trapping level of Cl_i^- is calculated to be 0.32 eV below VBM and therefore Cl_i^- should be a shallow acceptor in $\text{CH}_3\text{NH}_3\text{PbI}_2\text{Cl}$, in contrast to the relative deep (0/-) level of I_i^- (

$\varepsilon_{\text{VBM}} + 0.18$ eV) in $\text{CH}_3\text{NH}_3\text{PbI}_3$. Therefore, carrier trapping and recombination in $\text{CH}_3\text{NH}_3\text{PbI}_2\text{Cl}$ should be significantly reduced compared to those in $\text{CH}_3\text{NH}_3\text{PbI}_3$, which is consistent with the experimentally observed longer electron and hole diffusion lengths in $\text{CH}_3\text{NH}_3\text{PbI}_2\text{Cl}$ than in $\text{CH}_3\text{NH}_3\text{PbI}_3$.

IV. Conclusions

DFT calculations are performed to understand the exceptionally good carrier transport properties of $\text{CH}_3\text{NH}_3\text{PbI}_3$. The electronic structure, Born effective charge, dielectric constant, and defect properties of $\beta\text{-CH}_3\text{NH}_3\text{PbI}_3$ are calculated to provide comprehensive understanding of the material properties that affect carrier transport. Three factors are found to play important roles in carrier transport in $\text{CH}_3\text{NH}_3\text{PbI}_3$: (1) small electron and hole effective masses; (2) large Born effective charges and the resulting large static dielectric constant, which provides effective screening for charged defects and impurities. The low-temperature synthesis is also important for suppressing defect formation; (3) iodine interstitial is the only low-energy deep trap and non-radiative recombination centre among native point defects (including vacancies, interstitials, and antisites). However, the carrier trapping at the iodine interstitial should involve a kinetic barrier, which limits the trapping cross-section.

Defect properties in mixed halide $\text{CH}_3\text{NH}_3\text{PbI}_2\text{Cl}$ are calculated and compared with those of $\text{CH}_3\text{NH}_3\text{PbI}_3$. The alloying reduces the lattice constant and thus significantly increases the formation energies of interstitials, including the iodine interstitial. The introduction of Cl interstitials as a result of alloying cannot negate the benefit of suppressing other interstitial defects because (1) Cl_i^+

has a higher formation energy than that of I_i^+ in $\text{CH}_3\text{NH}_3\text{PbI}_2\text{Cl}$, which is already much higher than that of I_i^+ in $\text{CH}_3\text{NH}_3\text{PbI}_3$; Cl_i^- may partially compensate the reduction of $[\text{I}_i^-]$, but Cl_i^- is a shallow acceptor (shallower than I_i^-) and thus is not an effective hole trap. Therefore, alloying can significantly reduce carrier trapping and non-radiative recombination and explains the observed substantial improvement of transport properties in $\text{CH}_3\text{NH}_3\text{PbI}_2\text{Cl}$ compared to $\text{CH}_3\text{NH}_3\text{PbI}_3$.

The unique electronic structure, dielectric properties, and defect properties of halide perovskites used in solar cells are related to the chemistry of the ns^2 ion. (Pb^{2+} is a $6s^2$ ion.) Small effective masses for electrons and holes, large Born effective charges, large static dielectric constant, and the lack of defect-induced deep carrier traps have been found in other halides that contain ns^2 ions,^{18,19,20,21} where good transport properties have been reported.^{22,23} The understanding obtained in this work and our previous work on halides containing ns^2 ions provide the theoretical foundation for exploring this class of halides as high-performance electronic and optoelectronic materials.

Acknowledgements

The author is grateful for the stimulating discussion with David J. Singh. This work was supported by the Department of Energy, Basic Energy Sciences, Materials Sciences and Engineering Division.

Notes and references

^a Materials Science & Technology Division, Oak Ridge, TN 37831, USA.

- ¹ S. D. Stranks, G. E. Eperon, G. Grancini, C. Menelaou, M. J. P. Alcocer, T. Leijtens, L. M. Herz, A. Petrozza, and H. J. Snaith, *Science* **342**, 341 (2013).
- ² G. Xing, N. Mathews, S. Sun, S. S. Lim, Y. M. Lam, M. Grätzel, S. Mhaisalkar, T. C. Sum, *Science* **342**, 344 (2013).
- ³ C. C. Stoumpos, C. D. Malliakas, J. A. Peters, Z. Liu, M. Sebastian, J. Im, T. C. Chasapis, A. C. Wibowo, D. Y. Chung, A. J. Freeman, B. W. Wessels, and M. G. Kanatzidis, *Cryst. Growth Design* **13**, 2722 (2013).
- ⁴ L. Etgar, P. Gao, Z. Xue, Q. Peng, A. K. Chandiran, B. Liu, Md. K. Nazeeruddin, and M. Grätzel, *J. Am. Chem. Soc.* **134**, 17396 (2012).
- ⁵ I. Chung, B. Lee, J. He, R. P. H. Chang, and M. G. Kanatzidis, *Nature* **485**, 486 (2012).
- ⁶ M. M. Lee, J. Teuscher, T. Miyasaka, T. N. Murakami, H. J. Snaith, *Science* **338**, 643 (2012).
- ⁷ M. Liu, M. B. Johnson, and H. J. Snaith, *Nature* **501**, 395 (2013).
- ⁸ J. M. Ball, M. M. Lee, A. Hey, and H. J. Snaith, *Energy Environ. Sci.* **6**, 1739 (2013).
- ⁹ L. -Y. Huang and W. R. L. Lambrecht, *Phys. Rev. B* **88**, 165203 (2013).

- ¹⁰ J. Even, L. Pedesseau, J. -M. Jancu, and C. Katan, *J. Phys. Chem. Lett.* **4**, 2999 (2013).
- ¹¹ J. Even, L. Pedesseau, J. -M. Jancu, and C. Katan, *Phys. Stat. sol. RPL* **1**, 31 (2014).
- ¹² G. Giorgi, J. -I. Fujisawa, H. Segawa, and K. Yamashita, *J. Phys. Chem. Lett.* **4**, 4213 (2013).
- ¹³ E. Mosconi, A. Amat, Md. K. Nazeeruddin, M. Grätzel, and F. De Angelis, *J. Phys. Chem. C* **117**, 13902 (2013).
- ¹⁴ F. Brivio, A. B. Walker, and A. Walsh, *APL Mater.* **1**, 042111 (2013).
- ¹⁵ T. Baikie, Y. Fang, J. M. Kadro, M. Schreyer, F. Wei, S. G. Mhaisalkar, M. Graetzel, and T. J. White, *J. Mater. Chem. A* **1**, 5628 (2013).
- ¹⁶ C. C. Stoumpos, C. D. Malliakas and M. G. Kanatzidis, *Inorg. Chem.* **52**, 9019 (2013).
- ¹⁷ W. -J. Yin, T. Shi, and Y. Yan, *Appl. Phys. Lett.* **104**, 063903 (2014).
- ¹⁸ M. H. Du, *J. Appl. Phys.* **108**, 053506 (2010).
- ¹⁹ M. H. Du and D. J. Singh, *Phys. Rev. B* **81**, 144114 (2010).
- ²⁰ M. H. Du and D. J. Singh, *Phys. Rev. B* **82**, 045203 (2010).
- ²¹ K. Biswas, M. H. Du, and D. J. Singh, *Phys. Rev. B* **86**, 144108 (2012).
- ²² A. V. Churilov, G. Ciampi, H. Kim, L. J. Cirignano, W. M. Higgins, F. Olschner, and K. S. Shah, *IEEE Trans. Nucl. Sci.* **56**, 1875 (2009).

- ²³ S. Johnsen, Z. Liu, J. A. Peters, J.-H. Song, S. Nguyen, C. D. Malliakas, H. Jin, A. J. Freeman, B. W. Wessels, and M. G. Kanatzidis, *J. Am. Chem. Soc.* **133**, 10030 (2011).
- ²⁴ W. Kohn and L. J. Sham, *Phys. Rev.* **140**, A1133 (1965).
- ²⁵ J. P. Perdew, K. Burke, and M. Ernzerhof, *Phys. Rev. Lett.* **77**, 3865, (1996).
- ²⁶ J. Heyd, G. E. Scuseria, and M. Ernzerhof, *J. Chem. Phys.* **125**, 224106 (2006).
- ²⁷ S. Kümmel and L. Kronik, *Rev. Mod. Phys.* **80**, 3 (2008).
- ²⁸ P. E. Blöchl, *Phys. Rev. B* **50**, 17953 (1994).
- ²⁹ G. Kresse and J. Furthmüller, *Phys. Rev. B* **54**, 11169 (1996).
- ³⁰ G. Kresse and D. Joubert, *Phys. Rev. B* **59**, 1758 (1999).
- ³¹ S.-H. Wei, *Comput. Mater. Sci.* **30**, 337 (2004).
- ³² C. G. Van de Walle and J. Neugebauer, *J. Appl. Phys.* **95**, 3851 (2004).
- ³³ Applying SOC usually has very small effect on forces and therefore does not change the structure within the force convergence criterion used in this work. Previous test on TlBr shows only small changes in calculated Born effective charges, which are the derivatives of the forces.
- ³⁴ R. E. Cohen, *Nature (London)* **358**, 136 (1992).
- ³⁵ W. Zhong, R.D. King-Smith and D. Vanderbilt, *Phys. Rev. Lett.* **72**, 3618 (1994).
- ³⁶ M Posternak, R. Resta, and A. Baldereschi, *Phys. Rev. B* **50**, 8911 (1994).
- ³⁷ Ph. Ghosez, J. -P. Michenard, and X. Gonze, *Phys. Rev. B* **58**, 6224 (1998).
- ³⁸ K. Biswas and M. H. Du, *J. Appl. Phys.* **109**, 113518 (2011).
- ³⁹ J. M. Frost, K. T. Butler, F. Brivio, C. H. Hendon, M. van Schilfgaarde, and A. Walsh, *Nano Lett.* DOI: 10.1021/nl500390f.